

Substrate Metabolism- Driven Assembly of
High-Quality $\text{CdS}_x\text{Se}_{1-x}$ Quantum Dots in
Escherichia coli. Molecular Mechanisms and
Bio-Imaging Application

Li-Jiao Tian,^{*,†} Yuan Min,^{*,†} Wen-Wei Li,^{**,†} Jie-Jie Chen,^{**,†} Nan-Qing Zhou,[†] Ting-

Ting Zhu,[†] Dao-Bo Li,[†] Jing-Yuan Ma,[‡] Peng-Fei An,[§] Li-Rong Zheng,[§] Hai Huang,[†]

Yang-Zhong Liu,[†] Han-Qing Yu[†]

[†] CAS Key Laboratory of Urban Pollutant Conversion, Department of Applied
Chemistry, University of Science and Technology of China, Hefei, 230026, China

‡ Shanghai Synchrotron Radiation Facility, Shanghai Institute of Applied Physics,
Chinese Academy of Sciences, Shanghai, 201204, China

§Beijing Synchrotron Radiation Laboratory, Institute of High Energy Physics, Chinese
Academy of Science, Beijing, 100049, China

This supporting information contains 30-page document, including 5 tables, 19
figures, references and this cover page.

EXPERIMENTAL SECTION

SDS-PAGE and LC-MS/MS Analyses. To identify the capping proteins, the purified Bio-QDs were mixed with SDS-PAGE loading dye and electrophoresed on a 12% polyacrylamide SDS-PAGE gel. The images were captured under UV irradiation. According to the images, the Bio-QDs enriched band was identified and then cut for LC-MS/MS analysis. LC-MS/MS analysis was performed using Thermo-Dionex Ultimate 3000 HPLC system with a home-made fused silica capillary column (75 μm ID, 150 mm length; Upchurch, Oak Harbor, WA) packed with C-18 resin (300 Å, 5 μm , Varian, Lexington, MA). The peptides were separated using 120 min gradient elution at a flow rate 0.30 $\mu\text{L}/\text{min}$. Mobile phase A consisted of 0.1% formic acid, and mobile phase B consisted of 80% acetonitrile and 0.1% formic acid.

Cytotoxicity assays of Bio-QDs. The purified Bio-QDs were digested with proteinase K (100 $\mu\text{g}/\text{mL}$) at 37 °C for 6 h and then washed twice with Tris-HCl buffer to remove the capping proteins. The purified and treated Bio-QDs (after digestion with proteinase K) were further used for the viability assays in c231 cells. The cells were cultured in 5% CO_2 , 95% air incubator at 37 °C. Cells were seeded in 24-well plates with 8000 cells/well in 500 μL culture medium for 12 h for cell adhesion. The

culture medium was replaced with 500 μ L fresh medium containing different content of purified and treated Bio-QDs. After further incubation of the cells for 12 h, the medium was replaced with fresh culture medium and added with 3-(4,5-dimethylthiazol-2-yl)-2,5-diphenyltetra-zolium bromide (MTT) solution. After 4 h treatment, 100 μ L of lysis buffer was added. Another 4 h later, the liquid samples were collected and measured using a Bio-Rad 680 microplate reader at 490 nm absorbance. The IC_{50} values were calculated using GraphPad Prism software (version 6.01).

Adenosine triphosphate (ATP) detection. The ATP concentrations were measured using ATP assay kit (Beyotime Institute of Biotechnology, China) relying on a bioluminescence technique. 1 mL samples were collected and washed twice using ice-cold deionized water and then re-suspended in 1 mL lysis buffer. The re-suspended cells were disrupted by ultrasound (2 s with 5 s intervals, 100 repeats in all) on ice, and then centrifuged to extract ATP. The supernatant (20 μ L) was used to react with ATP assay mixture (100 μ L), and the ATP content was measured using a microplate reader.

RESULTS AND DISCUSSION

Linkage between Bio-QDs capping proteins and biocompatibility. To examine whether the biocompatibility of Bio-QDs is ascribed to the capping proteins, dose-response viabilities of c231 cells were measured. The cells were placed in a medium containing different concentrations of purified and proteinase K treated Bio-QDs. After 12-h incubations, the cells showed 70 % viability at an extremely high Bio-QDs dosage of 110 µg/mL (Figure S5), while the proteinase K digested Bio-QDs treated cells exhibited only 42 % viability at the same dosage. This result confirms that the biocompatibility of Bio-QDs was strongly dependent on the proteins capping.

Mechanism of glucose-facilitated Bio-QDs synthesis. The glucose-facilitated group showed a significantly higher level of ATP than the control (Figure S12a). Consistently, the expression of ATP (*atpA*: ATP synthase subunit alpha)¹ synthesis related genes were up-regulated in the glucose-fed group (Figure 4b). Dose of uncoupling agent 2,4-dinitrophenol (DNP: blocking ATP synthesis)² competitively

inhibited the Bio-QDs formation (Figure S13). All these results suggest an enhanced production of ATP in glucose metabolism, which favors the Bio-QDs fabrication.

The glucose addition not only diverted the Cd biotransformation towards $\text{CdS}_x\text{Se}_{1-x}$ formation, but also significantly accelerated the uptake of Cd and Se. In particular, the cellular Se contents of the glucose-facilitated group after 9-h incubation were more than 5-fold higher than that of the control (Figures S12b, c). Such enhanced Se bioaccumulation might also have contributed to the improved Bio-QDs synthesis. The distinctly higher Se-to-Cd ratio (mole-to-mole) of cells in the glucose-facilitated group (0.33) than in the control (0.074) also supports that different Cd compounds were formed in the two groups (Figure S12d).

Table S1. Proteins in Fluorescent Band using SDS-PAGE Separation and LC/MS/MS Identification

proteins
major outer membrane prolipoprotein Lpp
50S ribosomal protein L31
Acid stress chaperone HdeB
50S ribosomal subunit protein L28
50S ribosomal subunit protein L21
30S ribosomal subunit protein S10
DNA-binding protein HU-alpha
30s ribosomal subunit protein S18
30S ribosomal subunit protein S7
outer membrane protein A precursor
50S ribosomal subunit protein L27
50S ribosomal subunit protein L7/L12
Thioredoxin A
serine hydroxymethyltransferase
GroES, 10 Kd chaperone
Malate dehydrogenase
30S ribosomal subunit protein S9
putative outer membrane protein YiaT
50S ribosomal subunit protein L11
Protein yjgF
integration host factor subunit alpha
30S ribosomal protein S20
hypothetical protein SF0148
50S ribosomal protein L24
50S ribosomal subunit protein L19
30S ribosomal protein S6
50S ribosomal subunit protein L22
50s ribosomal protein I34

phosphocarrier protein HPr

heat shock protein 15

glutaredoxin 1

Table S2. Reported Bio-QDs synthesized by *Escherichia coli*

organism	method	intracellular / extracellular	obtained material	synthesis time	Ref.
<i>E. coli</i>	add NaBH ₄	Extracellular	CdTe	1-9 d	3
engineered <i>E. coli</i>	express phytochelatin synthase and / or metallothionein	Intracellular	CdSe/CdTe	6-12 h	4
engineered <i>E. coli</i>	express glutathione synthase	Intracellular	CdTe	24 h	5
<i>E. coli</i>	-	Intracellular	CdSe	4-32 h	6
<i>E. coli</i>	-	Intracellular	CdS	3 h	7
engineered <i>E. coli</i>	express phytochelatin synthase	Intracellular	CdS	4 h	8

Table S3. Se *K*-edge EXAFS Curve Fitting Parameters^a

sample	shell	<i>N</i>	<i>R</i> (Å)	σ^2 (Å ²)	ΔE_0 (eV)	<i>R</i> (%)
Se ^b	Se-Se	2	2.38 (1)	0.004 (1)	6.9 (4)	0.1
CdSe ^c	Se-Cd	4	2.62 (1)	0.005 (1)	2.8 (4)	0.1
Na ₂ SeO ₃ ^d	Se-O	3	1.70 (1)	0.002 (3)	8.9 (5)	0.7
Se-Met ^e	Se-C	6	1.96 (1)	0.002 (4)	8.7 (7)	0.9
	Se-O	2.2 (2)	1.72 (1)	0.003 (1)		
LB-CdSe ^f	Se-Se	0.9 (5)	2.37 (4)	0.004 (1)	9.7 (1)	0.2
	Se-Cd	0.6 (3)	2.72 (4)	0.006 (1)		
	Se-C	0.1 (1)	2.19 (3)	0.003 (1)		
	Se-O	0.1 (1)	1.51 (8)	0.003 (1)		
Glc-CdSe ^g	Se-Se	1.2 (5)	2.33 (1)	0.005 (3)	1.3 (8)	0.2
	Se-Cd	2.0 (4)	2.60 (1)	0.006 (1)		
	Se-C	0.2 (2)	2.01 (8)	0.003 (1)		
Glc-Se ^h	Se-Se	2.6 (2)	2.34 (2)	0.003 (1)	5.9 (9)	0.1
	Se-Cd	2.7 (4)	2.60 (2)	0.005 (1)		
purified Bio-QDs ⁱ	Se-Se	0.2 (3)	2.38 (3)	0.004 (1)	1.5 (8)	0.3
	Se-C	0.6 (6)	1.98 (4)	0.005 (2)		

^a*N*, coordination number; *R*, distance between absorber and backscatter atoms; σ^2 , Debye–Waller factor to account for both thermal and structural disorders; ΔE_0 , inner potential correction; *R* factor (%) indicates the goodness of the fit. Errors are given in brackets. S_0^2 was fixed to 0.8 as determined from CdSe standard fitting. Bold numbers indicate fixed coordination number (*N*) according to the crystal structure. ^b Fitting range: $3 \leq k$ (1/Å) ≤ 14.2 and $1.7 \leq R$ (Å) ≤ 2.5 . ^c Fitting range: $3 \leq k$ (1/Å) ≤ 12.5 and Fitting range: $1.7 \leq R$ (Å) ≤ 2.8 . ^d Fitting range: $4.0 \leq k$ (1/Å) ≤ 13.3 and $1 \leq R$ (Å) ≤ 1.7 . ^e Fitting range: $3.5 \leq k$ (1/Å) ≤ 13.6 and $1.3 \leq R$ (Å) ≤ 1.9 . ^f Fitting range: $3.1 \leq k$ (1/Å) ≤ 11 and $1.0 \leq R$ (Å) ≤ 2.7 . ^g Fitting range: $3.7 \leq k$ (1/Å) ≤ 12.2 and $1.0 \leq R$ (Å) \leq

3.1. ^h Fitting range: $4.4 \leq k (\text{Å}) \leq 13.6$ and $1.2 \leq R (\text{Å}) \leq 3.2$. ⁱ Fitting range: $3.7 \leq k (\text{Å}) \leq 12.8$ and $1.3 \leq R (\text{Å}) \leq 2.8$.

Table S4. Cd K-edge EXAFS Curve Fitting Parameters

Sample	Shell	N	R (Å)	σ^2 (Å ²)	ΔE_0 (eV)	R (%)
CdO ^b	Cd-O	6	2.32 (1)	0.008 (1)	1.0 (7)	1.5
CdS ^c	Cd-S	4	2.52 (1)	0.006 (1)	1.9 (5)	0.1
CdSe ^d	Cd- Se	4	2.63 (1)	0.006 (1)	3.0 (6)	0.1
Cd ₃ (PO ₄) ₂ ^e	Cd-O	6.6 (5)	2.28 (2)	0.011 (1)	3.3 (9)	0.3
	Cd- Se	0.4 (5)	2.68 (3)	0.006 (3)		
LB-CdSe ^f	Cd-S	0.2 (7)	2.50 (2)	0.006 (3)	7.9 (2)	0.4
	Cd-O	4.0 (2)	2.30 (1)	0.011 (2)		
	Cd- Se	1.2 (3)	2.63 (8)	0.006 (3)		
Glc-CdSe ^g	Cd-S	0.3 (8)	2.58 (8)	0.006 (3)	2.2 (2)	0.9
	Cd-O	2.5 (9)	2.23 (9)	0.011 (2)		
	Cd- Se	1.7 (3)	2.67 (5)	0.006 (3)		
Purified Bio-QDs ^h	Cd-S	0.5 (6)	2.49 (6)	0.006 (3)	9.4 (4)	0.2
	Cd-O	2.0 (4)	2.34 (8)	0.008 (2)		

^a N , coordination number; R , distance between absorber and backscatter atoms; σ^2 , Debye–Waller factor to account for both thermal and structural disorders; ΔE_0 , inner potential correction; R factor (%) indicates the goodness of the fit. Errors are given in brackets. S_0^2 was fixed to 0.97 as determined from CdSe standard fitting. Bold numbers indicate fixed coordination number (N) according to the crystal structure. ^b Fitting range: $3.0 \leq k$ (1/Å) ≤ 10.6 and $1.1 \leq R$ (Å) ≤ 2.3 . ^cFitting range: $3 \leq k$ (1/Å) ≤ 12 and $1.3 \leq R$ (Å) ≤ 2.5 . ^dFitting range: $3 \leq k$ (1/Å) ≤ 11 and $1.6 \leq R$ (Å) ≤ 2.8 . ^eFitting range: $3.0 \leq k$ (1/Å) ≤ 11.8 and $1.0 \leq R$ (Å) ≤ 2.4 . ^fFitting range: $3.2 \leq k$ (1/Å) ≤ 10.6 and

$1.3 \leq R (\text{\AA}) \leq 2.8$. ^aFitting range: $3.0 \leq k (\text{\AA}) \leq 10.6$ and $1.2 \leq R (\text{\AA}) \leq 2.8$. ^bFitting range: $3.0 \leq k (\text{\AA}) \leq 10.6$ and $1.1 \leq R (\text{\AA}) \leq 2.9$.

Table S5. Primer Sequences for Quantitative RT-PCR

Gene	Direction	Primer
<i>rrsG</i> ⁹	Forward	5'-TAT TGC ACA ATG GGC GCA AG-3'
	Reverse	5'-ACT TAA CAA ACC GCC TGC GT-3'
<i>zwf</i>	Forward	5'-GGA ACG ACC ATC ACG GGT AAT C-3'
	Reverse	5'-ACG AAG TGG AAG AAG CCT GGA A-3'
<i>atpA</i>	Forward	5'-ACG CTG ACC ACG ACC GAT TG-3'
	Reverse	5'-ACG ACG GCT TCT CTG CTG TAG-3'
<i>gshA</i>	Forward	5'-ACC GCA CAG TTC CCG TTA CC-3'
	Reverse	5'-AAG CAG GCA ACC AGT TCA TCA C-3'
<i>grxA</i>	Forward	5' - GTT CGG GTT GCC CTT ACT- 3'
	Reverse	5' - GGT TTA CCT GCC TTT TGT TG - 3'
<i>trxA</i>	Forward	5'-TCC CGA CTC TGC TGC TGT TC-3'
	Reverse	5'-GCC AGG TTA GCG TCG AGG AA-3'
<i>soxR</i>	Forward	5'-CGT CCC AAT GGC GAG AAG AGT-3'
	Reverse	5'-GGG TTA CGC AAC GGG CAA TC-3'

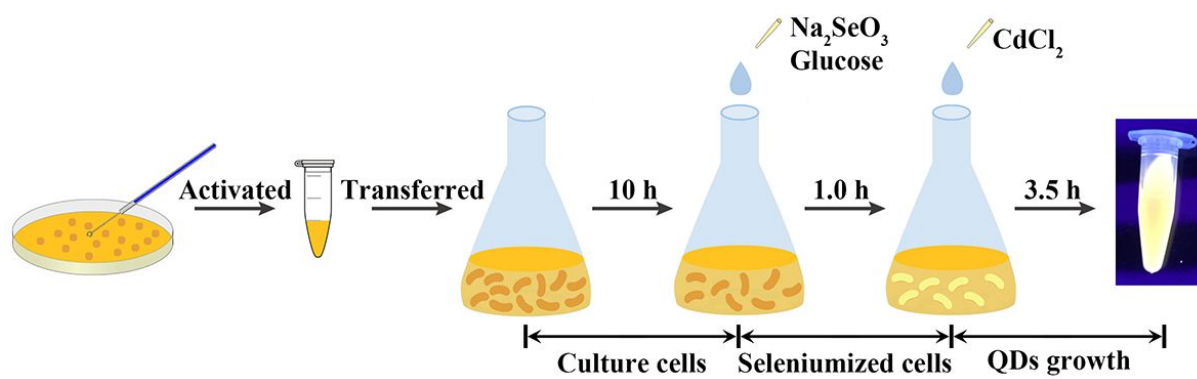


Figure S1. Diagram of operating procedures for Bio-QDs synthesis.

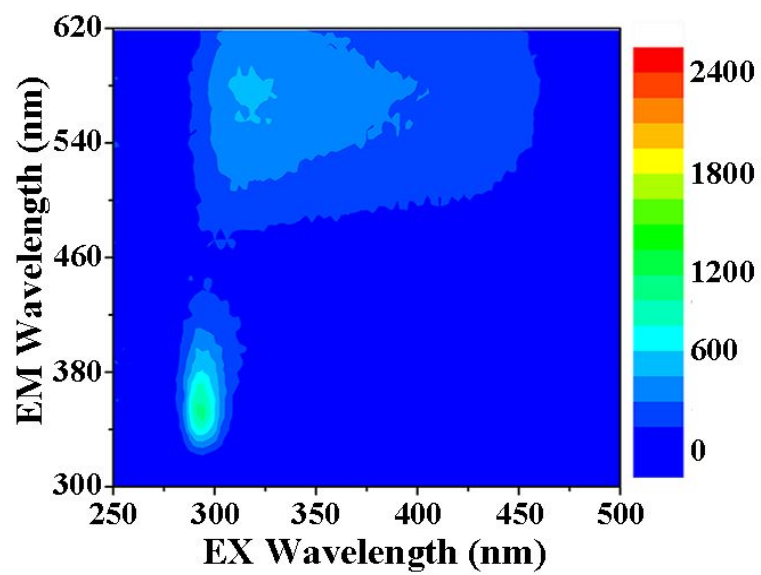


Figure S2. EEM fluorescence spectrum of the cells treated with 1 mM Na_2SeO_3 and 6 mM CdCl_2 for 3.5 h.

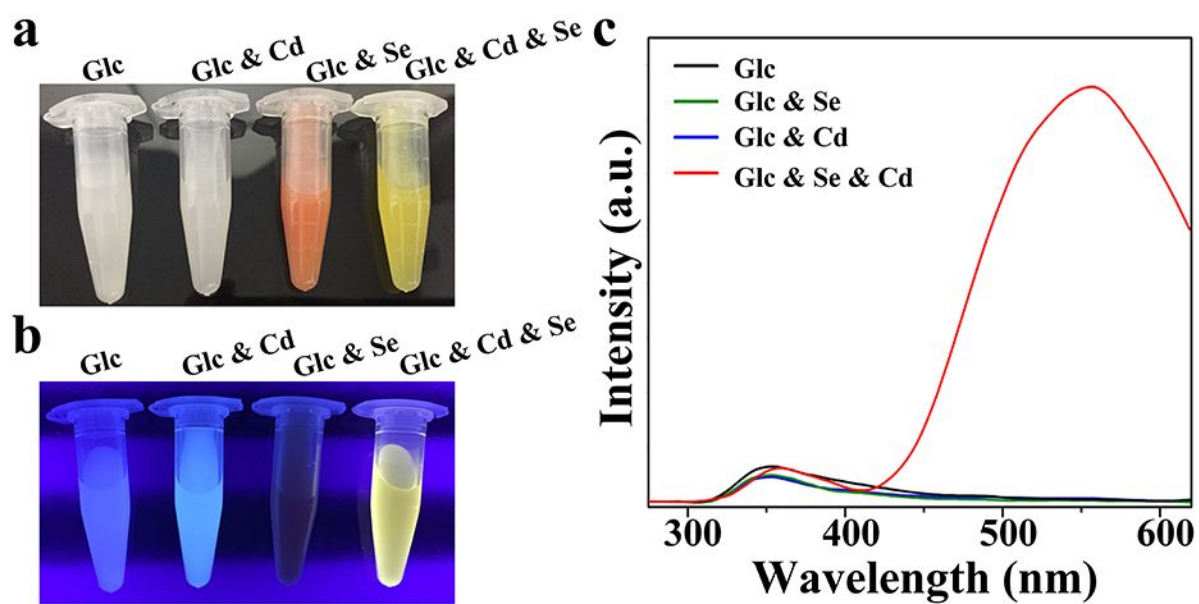


Figure S3. Optical images of treated *E. coli* cells under sunlight (a) and UV irradiation (b). (c) Fluorescence spectra of cells excited by a 310-nm wavelength. The culture medium was all added with glucose (Glc) but with different dosage scheme of Se and Cd.

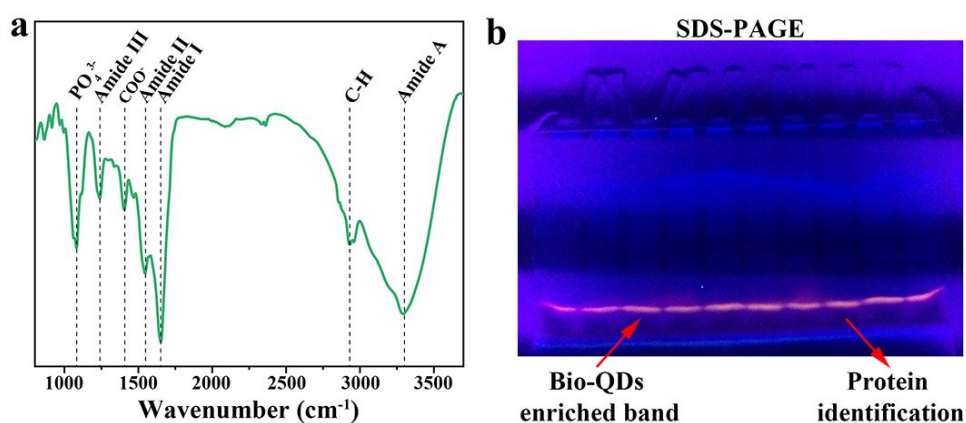


Figure S4. Surface chemical properties of the Bio-QDs. (a) FTIR spectrum of the purified Bio-QDs. (b) SDS-PAGE gel of the purified Bio-QDs had a fluorescent band corresponding to QDs. Cut the fluorescent band and then analyzed by LC-MS/MS to identify the proteins.

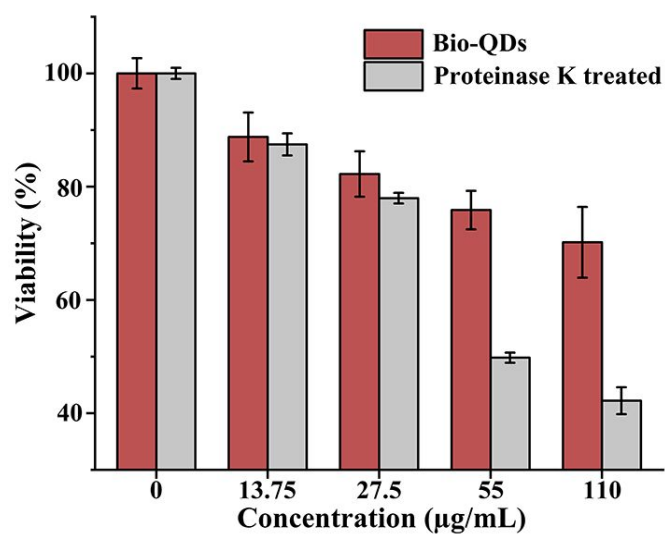


Figure S5. Dose-responsive viability of cancer cell line MDA-MB-231 in the medium spiked with Bio-QDs or proteinase K treated Bio-QDs.

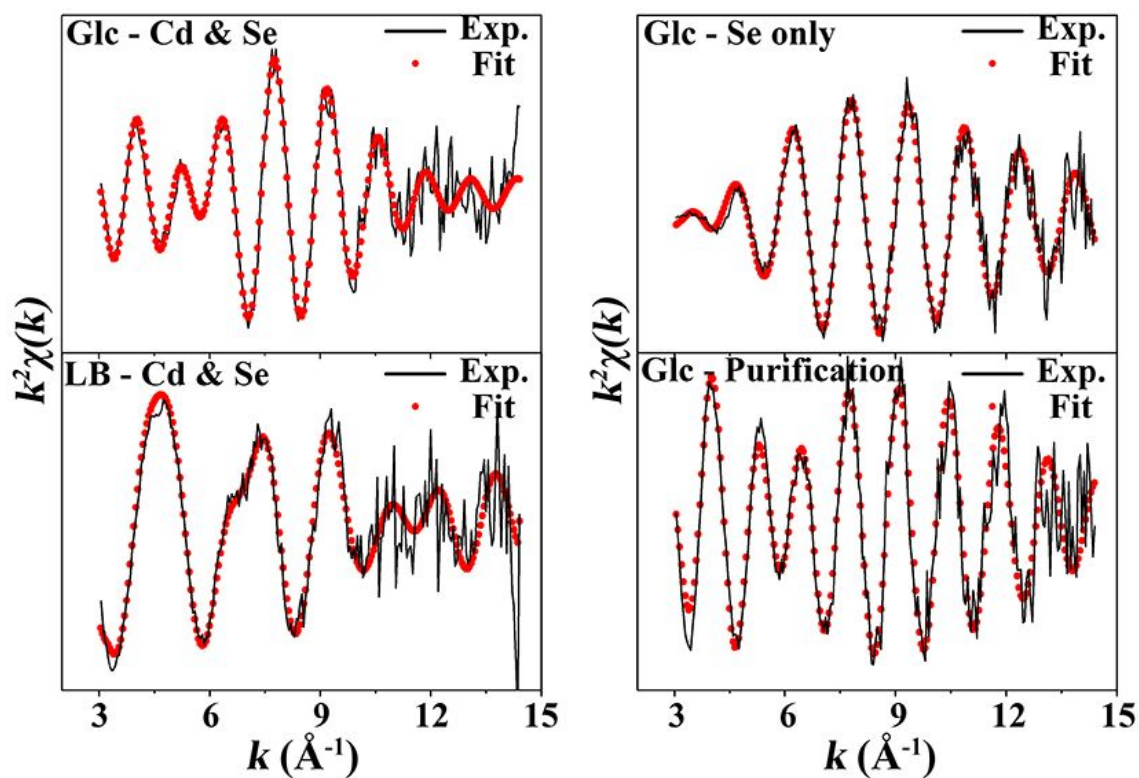


Figure S6. Se *K*-edge EXAFS analysis of the samples in *k* spaces. The theoretical signal (red circle) superimposed on the experimental one (black line). Measured spectra matched very well with the calculated results. The best-fit parameters are shown in Table S3.

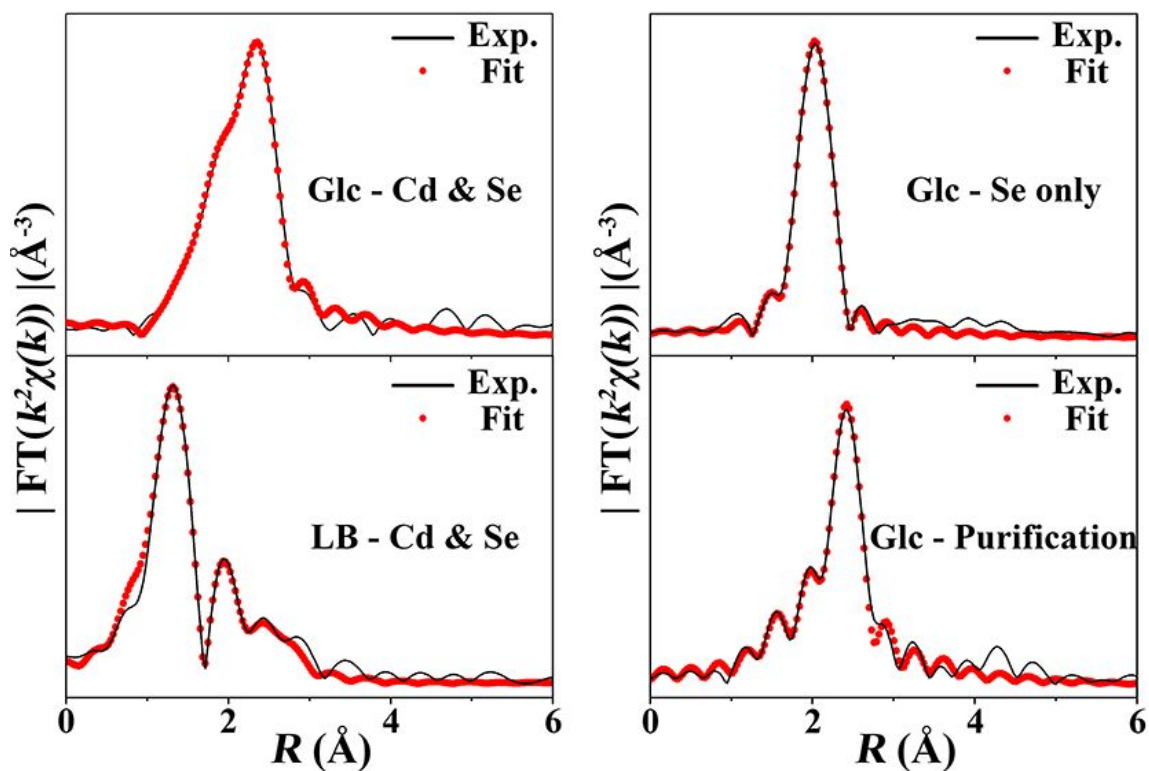


Figure S7. Se *K*-edge EXAFS analysis of the samples in *R* spaces. The theoretical signal (red circle) superimposed on the experimental one (black line). Measured spectra matched very well with the calculated results. The best-fit parameters are shown in Table S3.

The normalized Se *K*-edge EXAFS analysis shows that the Glc & Se only group showed a characteristic peak of Se-Se (Figures S6 and S7). Fitting of the spectra curves also validate the shift of dominant inorganic Se species from Na_2SeO_3 to Se-Se in the presence of glucose (Table S3).

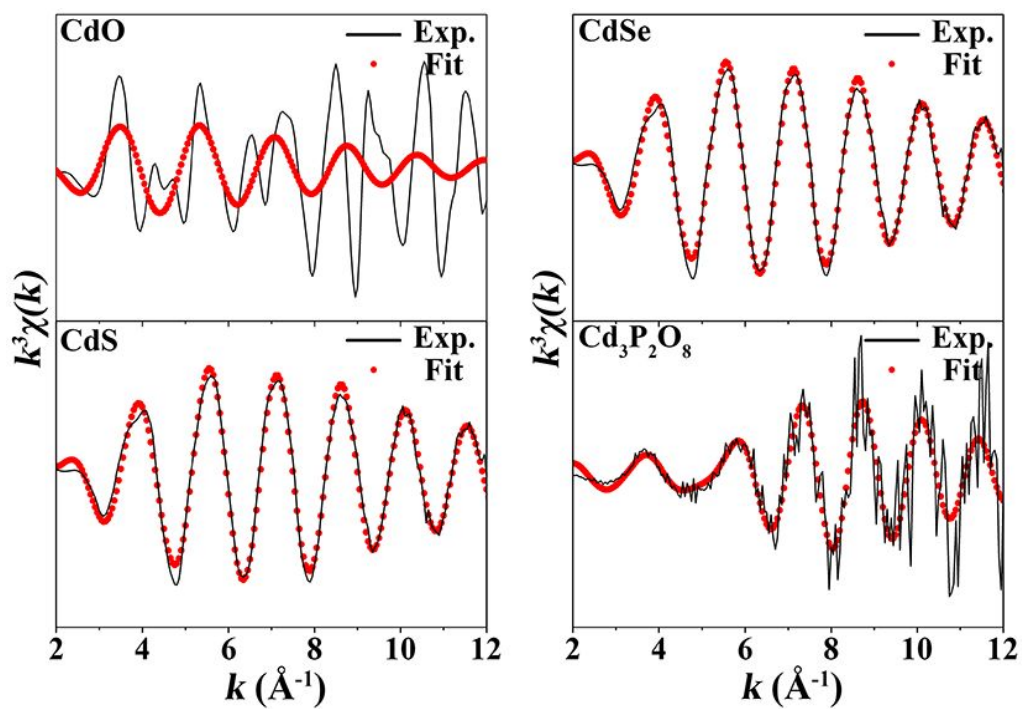


Figure S8. Cd *K*-edge EXAFS spectra in *R* space for CdO, CdS, CdSe and $\text{Cd}_3(\text{PO}_4)_2$ standards. Measured and calculated spectra matched very well with the standards. The best-fit parameters are shown in Table S4.

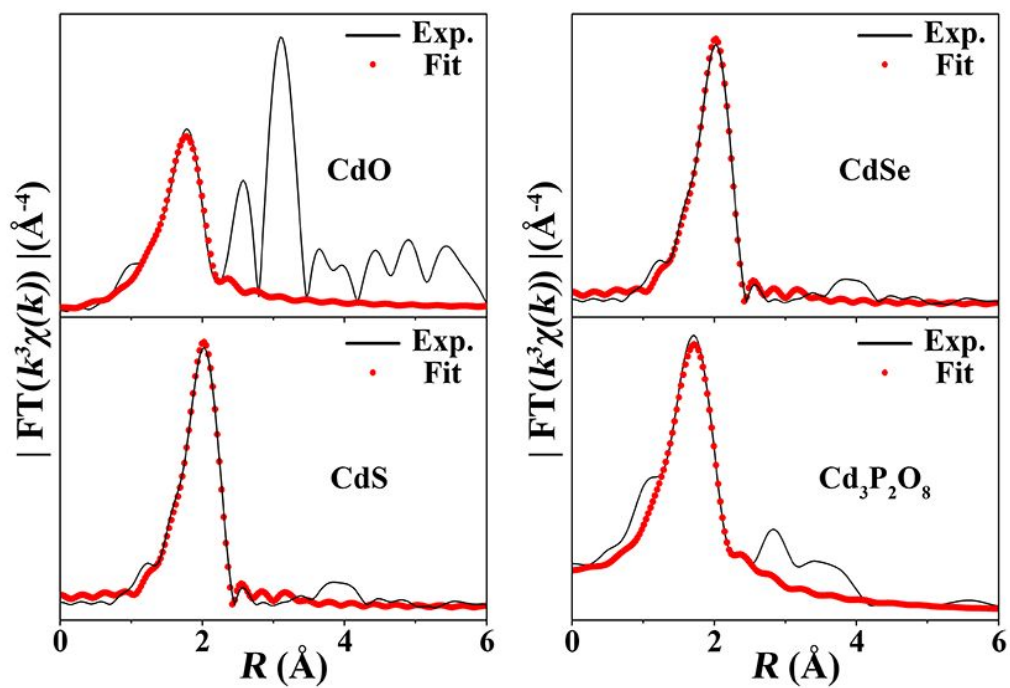


Figure S9. Fourier-transformed magnitudes of Cd *K*-edge EXAFS spectra in *R* space for CdO, CdS, CdSe and Cd₃(PO₄)₂ standards. Measured and calculated spectra matched very well with the standards. The best-fit parameters are shown in Table S4.

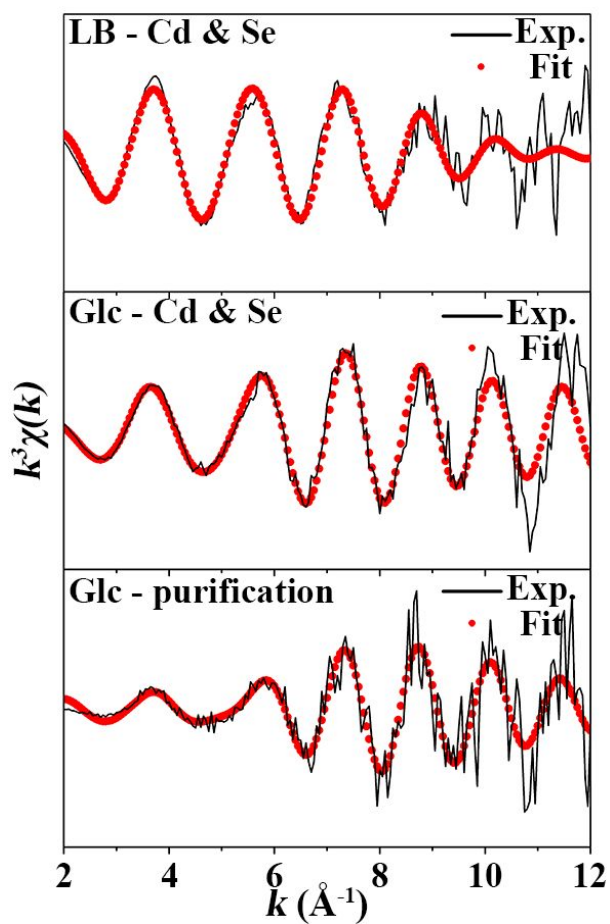


Figure S10. Cd K -edge EXAFS analysis of the samples in k spaces. The theoretical signal (red circle) superimposed on the experimental one (black line). Measured spectra matched very well with the calculated results. The best-fit parameters are shown in Table S4

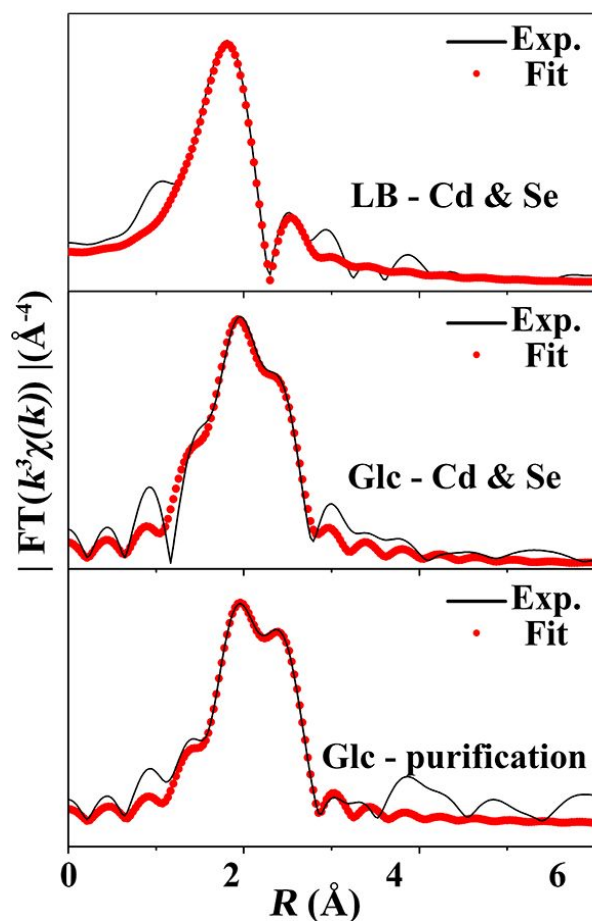


Figure S11. Fourier-transformed magnitudes of Cd *K*-edge EXAFS analysis of the samples in *R* space. The theoretical signal (red circle) superimposed on the experimental one (black line). Measured spectra matched very well with the calculated results. The best-fit parameters are shown in Table S4.

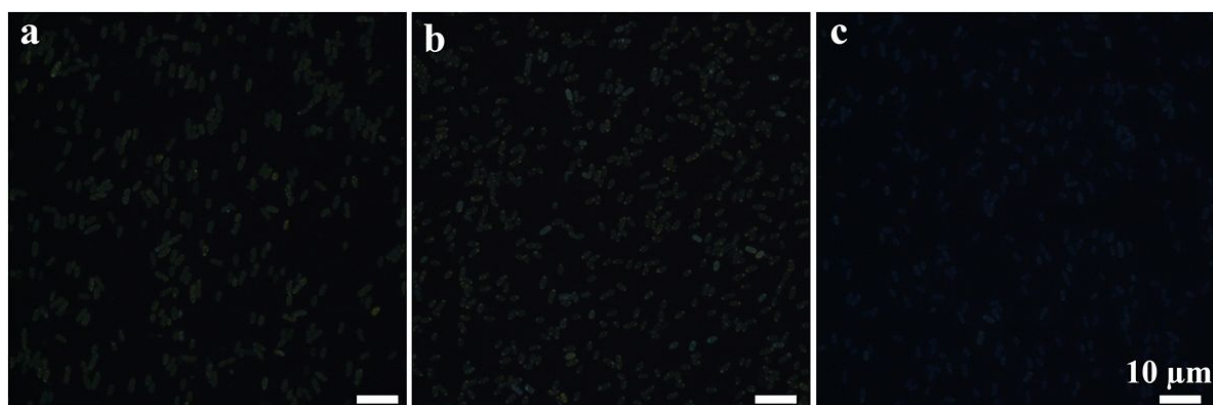


Figure S12. Fluorescence microscopic images of the *E. coli* cells co-incubated with 0.5 mM glutathione synthesis inhibitor (a) buthionine sulfoximine (BSO), (b) 50 μ M NADPH synthesis inhibitor diphenylene iodonium, and (c) 0.1 mM ATP synthesis blocker 2,4-dinitrophenol (DNP).

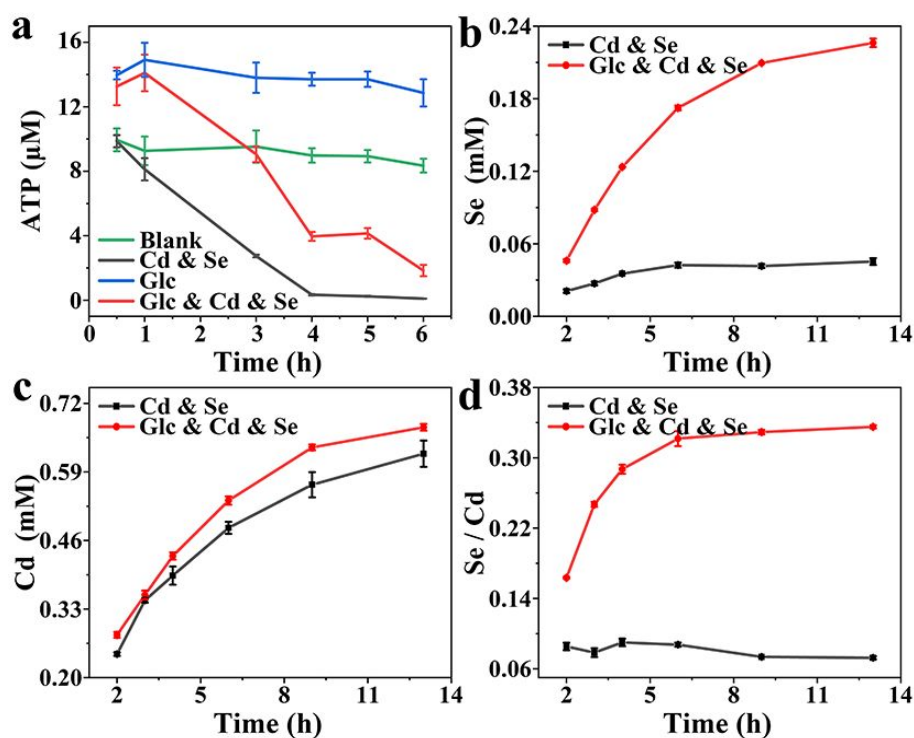


Figure S13. Impact of glucose on the accumulation of intracellular (a) adenosine triphosphate (ATP), (b) Se element, (c) Cd element in treated cells over synthesis time. (c) The intracellular Se-to-Cd ratio (mole-to-mole) was plotted based on (b) and (c). The biosynthesis process contains two stages: cell-seleniumized (within 1 h) and Cd-binding crystallization (after 1 h).

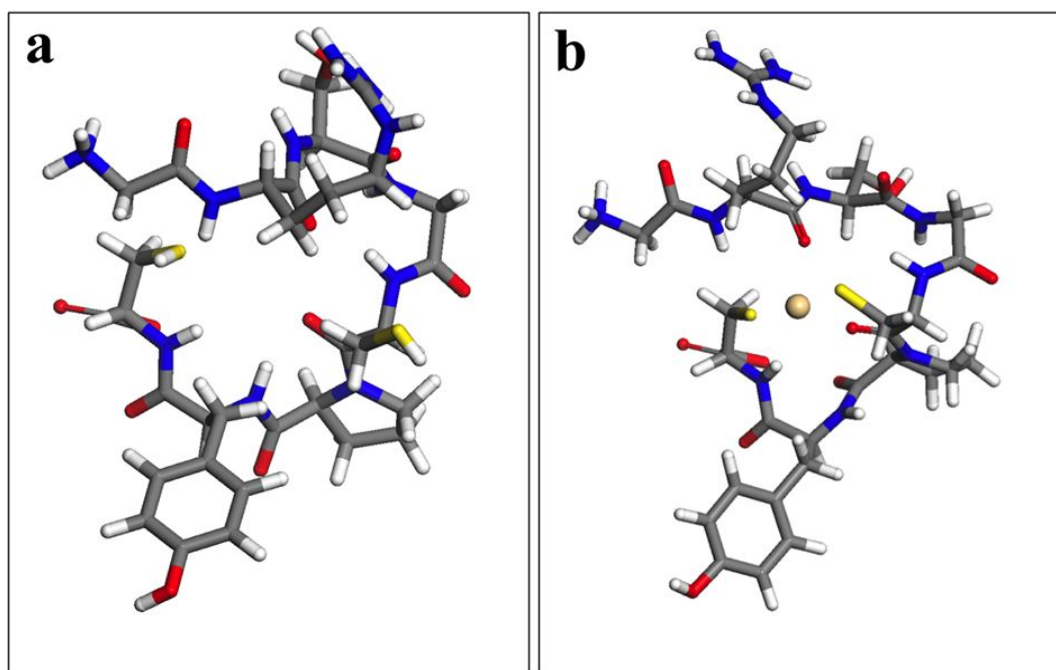


Figure S14. (a) Cysteine site of glutaredoxin (GRX). (b) Energy-minimized structures of GRX_{site}-Cd²⁺ complexes.

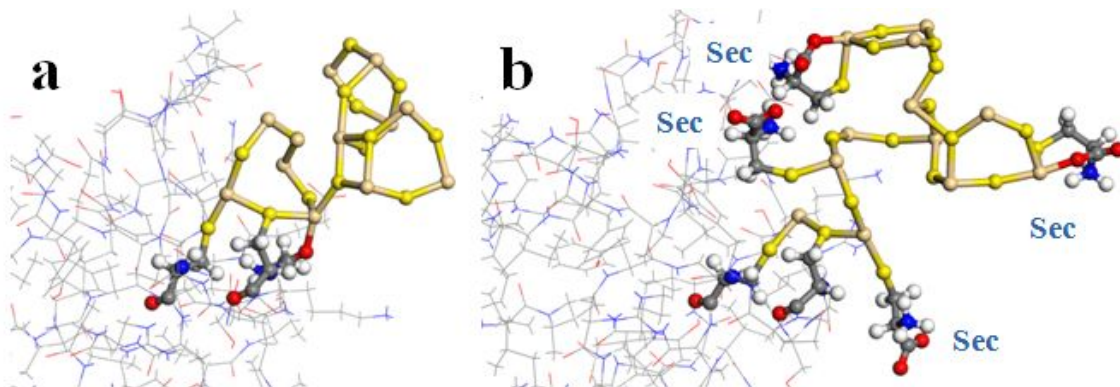


Figure S15. CdSe QDs generation in GRX (a) and GRX coupled with Sec ligands (b).

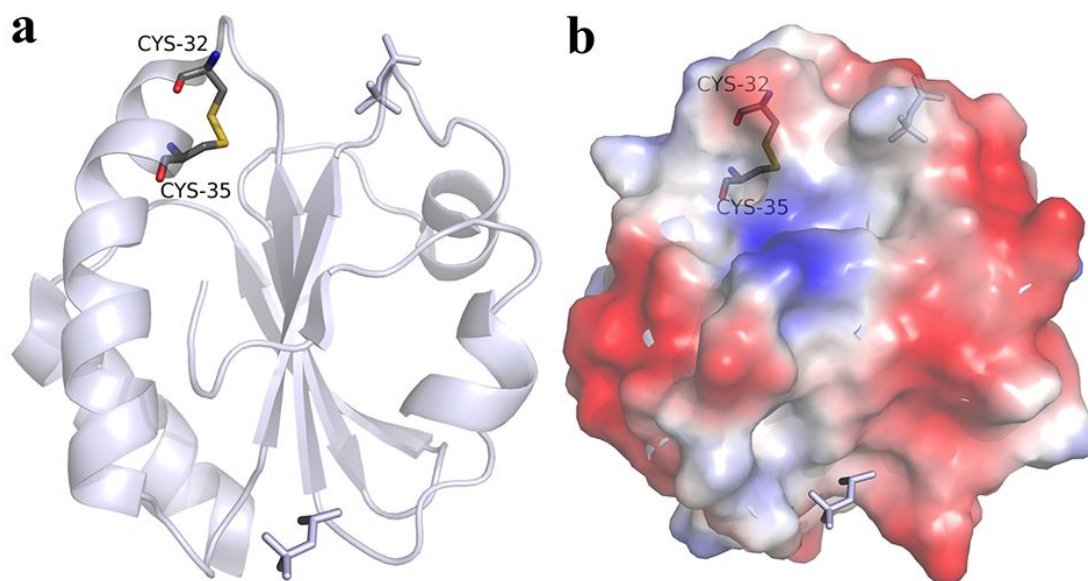


Figure S16. Thioredoxin structure and surface charge distribution. (a) Locations of Cys amino acids in *Escherichia coli* TRX (PDB ID: 2H6X). (b) Charge distribution on the protein surface (red: negatively charged surface, blue: positively-charged surface).

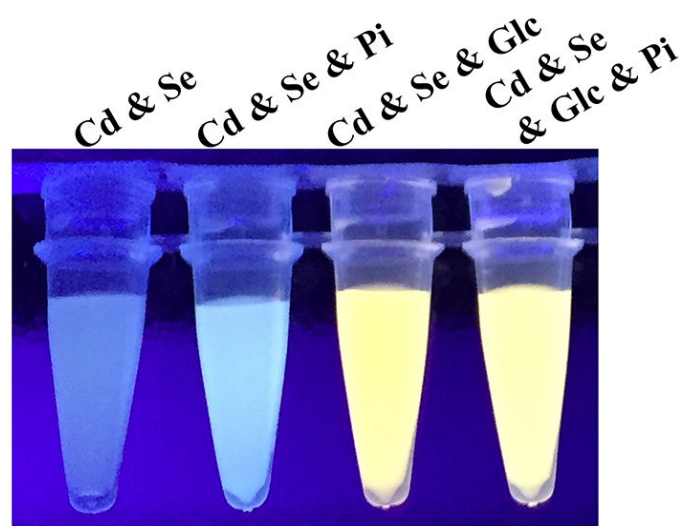


Figure S17. Optical images of the treated cells under UV irradiation. Impacts of glucose (Glc) and phosphates (Pi) on the optical properties of cells incubated with 1 mM Na_2SeO_3 and 6 mM CdCl_2 for 3.5 h.

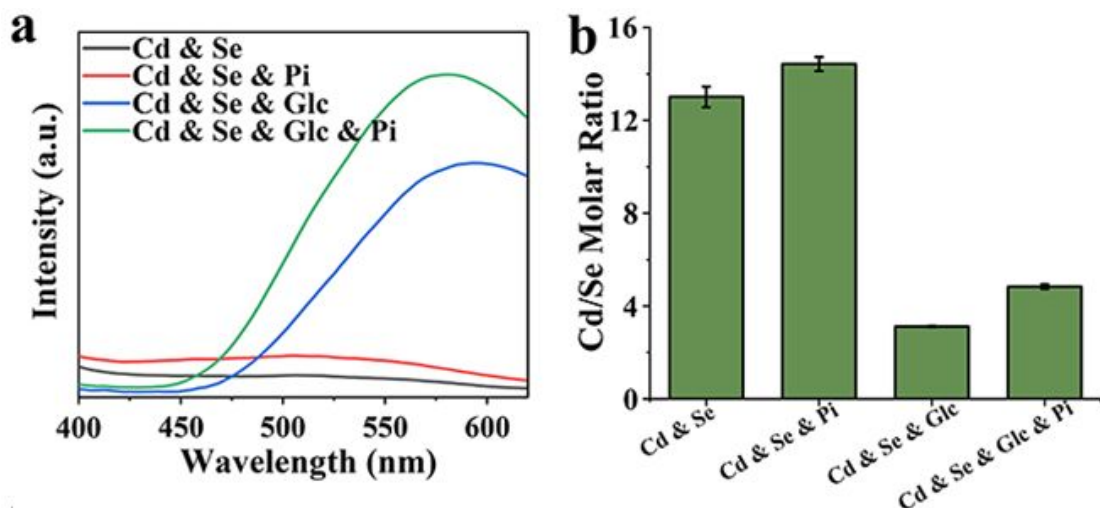


Figure S18. Impacts of glucose (Glc) and phosphates (Pi) on the optical properties of the cells incubated with 1 mM Na_2SeO_3 and 6 mM CdCl_2 for 3.5 h. (a) Emission fluorescence spectra of the treated cells with 310-nm excitation wavelength. (b) Cd/Se ratio of the purified Bio-QDs synthesized under different conditions.

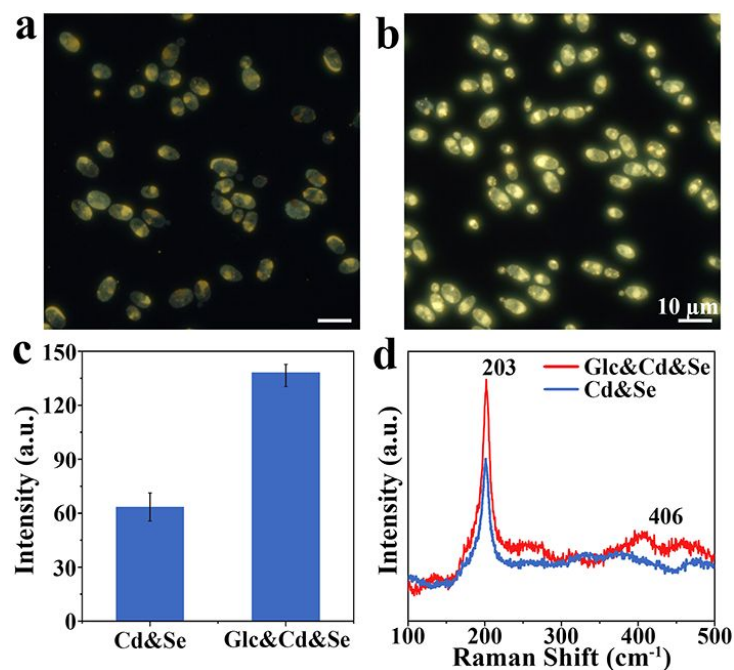


Figure S19. Fluorescence images of 1 mM Na_2SeO_3 and 6 mM CdCl_2 treated *C. utilis* WSH02-08 cells, which were incubated without glucose (a) or with glucose (b). (c) Intracellular mean fluorescence intensity shows the fluorescence changes of the Bio-QDs after glucose addition. (d) *In situ* micro-Raman spectrum (excited at 532 nm) of the synthesized *C. utilis* WSH02-08 with glucose.

REFERENCES

1. Morales-Rios, E.; Montgomery, M. G.; Leslie, A. G.; Walker, J. E., Structure of ATP Synthase from *Paracoccus denitrificans* Determined by X-ray Crystallography at 4.0 Å Resolution. *Proc. Natl. Acad. Sci. U. S. A.* **2015**, *112*, 13231-13236.
2. Miller, E. L.; Nason, S. L.; Karthikeyan, K. G.; Pedersen, J. A., Root Uptake of Pharmaceuticals and Personal Care Product Ingredients. *Environ. Sci. Technol.* **2016**, *50*, 525-541.
3. Bao, H.; Lu, Z.; Cui, X.; Qiao, Y.; Guo, J.; Anderson, J. M.; Li, C. M., Extracellular Microbial Synthesis of Biocompatible CdTe Quantum Dots. *Acta Biomater.* **2010**, *6*, 3534-3541.
4. Park, T. J.; Lee, S. Y.; Heo, N. S.; Seo, T. S., *In Vivo* Synthesis of Diverse Metal Nanoparticles by Recombinant *Escherichia coli*. *Angew. Chem. Int. Edit.* **2010**, *49*, 7019-7024.
5. Monras, J. P.; Diaz, V.; Bravo, D.; Montes, R. A.; Chasteen, T. G.; Osorio-Roman, I. O.; Vasquez, C. C.; Perez-Donoso, J. M., Enhanced Glutathione Content Allows

the *In Vivo* Synthesis of Fluorescent Cdte Nanoparticles by *Escherichia coli*. *PLoS*

One **2012**, *7*, e48657.

6. Yan, Z.; Qian, J.; Gu, Y.; Su, Y.; Ai, X.; Wu, S., Green Biosynthesis of Biocompatible Cdse Quantum Dots in Living *Escherichia coli* Cells. *Mater. Res. Express* **2014**, *1*, 015401.

7. Sweeney, R. Y.; Mao, C.; Gao, X.; Burt, J. L.; Belcher, A. M.; Georgiou, G.; Iverson, B. L., Bacterial Biosynthesis of Cadmium Sulfide Nanocrystals. *Chem. Biol.* **2004**, *11*, 1553-1559.

8. Kang, S. H.; Bozhilov, K. N.; Myung, N. V.; Mulchandani, A.; Chen, W., Microbial Synthesis of CdS Nanocrystals in Genetically Engineered *E. coli*. *Angew. Chem. Int. Edit.* **2008**, *47*, 5186-5189.

9. Lee, J. H.; Regmi, S. C.; Kim, J. A.; Cho, M. H.; Yun, H.; Lee, C. S.; Lee, J., Apple Flavonoid Phloretin Inhibits *Escherichia coli* O157:H7 Biofilm Formation and Ameliorates Colon Inflammation in Rats. *Infect. Immun.* **2011**, *79*, 4819-4827.